AGU PUBLICATIONS

JGR

Journal of Geophysical Research: Solid Earth

RESEARCH ARTICLE
10.1002/2016JB013209

Key Points:
- FeAl-bearing phase D undergoes a two-stage spin transition of iron at high pressure
- The spin transitions are associated with an increase in density and a decrease in bulk modulus and bulk sound velocity
- The dense low-spin FeAl-bearing phase D can contribute to observed seismic anisotropies and heterogeneities in the middle-lower mantle

Supporting Information:
- Supporting Information S1

Correspondence to:
X. Wu and J.-F. Lin,
wuxiang@cug.edu.cn;
afu@jsg.utexas.edu

Citation:
Wu, X., Y. Wu, J.-F. Lin, J. Liu, Z. Mao, X. Guo, T. Yoshino, C. McCammon, V. B. Prakapenka, and Y. Xiao (2016), Two-stage spin transition of iron in FeAl-bearing phase D at lower mantle, *J. Geophys. Res. Solid Earth*, *121*, doi:10.1002/2016JB013209.

Received 26 MAY 2016
Accepted 31 AUG 2016
Accepted article online 4 SEP 2016

Two-stage spin transition of iron in FeAl-bearing phase D at lower mantle

Xiang Wu[1,2], Ye Wu[2], Jung-Fu Lin[3,4], Jin Liu[3], Zhu Mao[5], Xinzhuan Guo[1,6], Takashi Yoshino[6], Catherine McCammon[7], Vitali B. Prakapenka[8], and Yuming Xiao[9]

[1]State Key Laboratory of Geological Processes and Mineral Resources, China University of Geosciences, Wuhan, China, [2]Key Laboratory of Orogenic Belts and Crustal Evolution, MOE, School of Earth and Space Sciences, Peking University, Beijing, China, [3]Department of Geological Sciences, The University of Texas at Austin, Austin, Texas, USA, [4]Center for High Pressure Science and Technology Advanced Research, Shanghai, China, [5]School of Earth and Space Sciences, University of Science and Technology of China, Hefei, China, [6]Institute for Study of the Earth's Interior, Okayama University, Tottori, Japan, [7]Bayerisches Geoinstitut, Universität Bayreuth, Bayreuth, Germany, [8]Center for Advanced Radiation Sources, University of Chicago, Chicago, Illinois, USA, [9]HPCAT, Geophysical Laboratory, Carnegie Institution of Washington, Washington, District of Columbia, USA

Abstract Hydrous magnesium silicate phase D plays a key role in the transport of water from the upper to the lower mantle via subducted slabs. Here we report pressure dependence hyperfine and lattice parameters of FeAl-bearing phase D up to megabar pressures using synchrotron nuclear forward scattering and X-ray diffraction in a diamond anvil cell at room temperature. FeAl-bearing phase D undergoes a two-stage high-spin to low-spin transition of iron for Fe^{2+} at 37–41 GPa and for Fe^{3+} at 64–68 GPa. These transitions are accompanied by an increase in density and a significant softening in the bulk modulus and bulk velocity at their respective pressure range. The occurrence of the dense low-spin FeAl-bearing phase D with relatively high velocity anisotropies in deep-subducted slabs can potentially contribute to small-scale seismic heterogeneities in the middle-lower mantle beneath the circum-Pacific area.

1. Introduction

A recent study of hydrous ringwoodite inclusion in diamond from the transition zone suggests that the transition zone is wet [*Pearson et al*., 2014], and high-pressure experimental investigations on phase H ($MgSiH_2O_4$) have implied that the lower mantle may be similarly hydrated [*Nishi et al*., 2014], but we do not have good constraints on the amount of hydrogen in the lower mantle [*Nestola and Smyth*, 2016]. The surface water can be transported to the deep Earth via subducted slabs, and with its strong effects on the chemical and physical properties of mantle materials, which have significant implications for understanding geochemical, geophysical, and geodynamical processes in the Earth's mantle [*Hirschmann*, 2006; *Faccenda*, 2014]. Water carriers and their capacities therefore have been studied extensively in the MgO-SiO_2-H_2O system, where dense hydrous magnesium silicates (DHMSs) are primary candidates for water reservoirs. Phase D, a classic DHMS with a wide pressure-temperature (*P-T*) stability range [*Shieh et al*., 1998; *Shinmei et al*., 2008; *Tsuchiya*, 2013; *Nishi et al*., 2014; *Ghosh and Schmidt*, 2014; *Pamato et al*., 2015], may carry water from the upper to lower mantle. Thus, the properties of phase D, including structural stability, sound velocity, electronic conductivity, texture, and melting, have been used, for example, in discussions of water recycling, buoyancy of deep-subducted slabs, and seismic velocity anomalies in the uppermost-to-middle lower mantle [*Lawrence and Wysession*, 2006; *Chang et al*., 2013; *Rosa et al*., 2012, 2013a, 2013b; *Ghosh and Schmidt*, 2014].

Phase D with chemical variations of 10–18 wt % H_2O contents crystallizes in a trigonal phase ($P\bar{3}m$ and $Z = 1$) consisting of alternating layers of MgO_6 and SiO_6 octahedra stacked along the *c* axis and disordered OH^- located between octahedra in the MgO_6 layer [*Yang et al*., 1997; *Xue et al*., 2008]. Fe and Al elements as the high abundance in deep Earth exist in mantle minerals, such as garnet and bridgmanite. Phase D can also incorporate significant amounts of Fe and Al [*Litasov et al*., 2007, 2008; *Rosa et al*., 2012; *Chang et al*., 2013; *Ganskow and Langenhorst*, 2014], where Al^{3+} substitutes for Si^{4+}, Fe^{2+} does for Mg, and Fe^{3+} may occupy Si and Mg sites [*Ganskow and Langenhorst*, 2014]. Available data demonstrate that the $Fe^{3+}/\Sigma Fe$ ratio of Fe-bearing phase D is 0.60–0.94 determined by conventional Mössbauer spectroscopy and electron energy loss spectroscopy, and iron is not involved in water-substitution mechanisms [*Chang et al*., 2013; *Ganskow and Langenhorst*, 2014]. Electronic high-spin (HS) to low-spin (LS) transition of iron has been reported to occur

in a number of candidate mantle minerals, such as ferropericlase and bridgmanite, significantly affecting the physical and chemical properties of the hosts [*Lin et al*., 2013]. Indeed Chang et al. observed a HS-to-LS crossover of Fe^{3+} in $MgSi_{1.5}Fe3^{+}$ $0.15Al_{0.3}H_{2.6}O_6$ between 40 GPa and 65 GPa, resulting in a softening of the bulk sound velocity and thus providing an alternate explanation for small-scale seismic scatters in the middle-lower mantle [*Chang et al*., 2013]. But the property of LS-Fe^{3+} phase D is of large uncertainty, for example, the larger error in the bulk modulus of 253(30) GPa [*Chang et al*., 2013]. We have no information about electric structure of Fe^{2+} in FeAl-bearing phase D under compression, limiting further discussion on the combinational effect of ferric and ferrous irons and its implications. In FeAl-bearing phase D, both Fe^{2+} and Fe^{3+} are isolated onto octahedral sites, whose spin states at high pressure are expected to shed light on the issue of the nature of mixed-valence iron spin transition at multiple sites in other mantle phases such as FeAl-bearing bridgmanite and postperovskite. In addition, pressure-induced hydrogen bond symmetrization in phase D is still debated without the direct experimental evidences, like the data of AlOOH from high-pressure neutron diffraction [*Sano-Furukawa et al*., 2008]. Therefore, the combined effects of Fe, Al, and H on the structural and physical properties of phase D remain elusive but can help improve the understanding of deep water reservoirs and geophysical observations in the Earth's interior.

Here we have used synchrotron nuclear forward scattering (NFS) with high-energy resolution and single-crystal X-ray diffraction (XRD) with high accuracy to explore pressure-induced structural changes of high-quality single-crystal phase D samples, both FeAl free ($Mg_{1.14}Si_{1.73}H_{2.81}O_6$) and FeAl bearing ($Mg_{0.89}Fe_{0.11}Al_{0.37}Si_{1.55}H_{2.65}O_6$). Our results up to megabar pressures reveal the oxidation states, spin states, and local environments of iron in FeAl-bearing phase D, which strongly affect the elasticity and the hydrogen bond properties of FeAl-bearing phase D relative to those of FeAl-free phase D. These findings have significant implications for the storage of water and seismic velocity anomalies in the uppermost-to-middle lower mantle.

2. Methods

2.1. Sample Synthesis and Characterization

High-quality single-crystal FeAl-free phase D labeled 5K2321 and FeAl-bearing phase D labeled 5K2209 were synthesized using a USSA-5000 Kawai-type apparatus at the Institute for Study of the Earth's Interior, University of Okayama, Japan. In the run of the 5K2321 experiment, specific synthesis conditions were the same as those of the reference [*Guo and Yoshino*, 2013]. The recovered samples were colorless single crystals with large grain sizes of ~300 μm. In the run of the 5K2209 experiment, the starting material was a mixture of $Mg(OH)_2$, SiO_2, $Al(OH)_3$, and $^{57}Fe_2O_3$ with a molar ratio of 1.0:1.5:0.3:0.075. It was loaded into a double capsule assembly consisting of an unsealed inner Re capsule and a sealed outer Pt capsule. The sample assembly was compressed up to 21 GPa and then heated to 1200°C for 12 h. The recovered samples were light green single crystals with large grain sizes of ~200 μm. Sample characterization was performed at ambient conditions using X-ray diffraction (XRD), Raman spectroscopy, conventional Mössbauer spectroscopy (MS), and electron microscope analysis (EMPA). Raman spectra of 10 grains picked randomly from the 5K2209 or 5K2321 batches were the same and in agreement with those of phase D reported by *Xue et al*. [2008]. Electron microprobe results also indicated that samples were chemically homogeneous. The crystal structure at ambient conditions was determined to be hexagonal phase ($P\bar{3}m$ and $Z = 1$) with lattice constants of $a = 4.7855(1)$ Å, $c = 4.3212(4)$ Å, and $V = 85.711(7)$ Å^3 for FeAl-bearing phase D and $a = 4.7533(2)$ Å, $c = 4.3545(5)$ Å, and $V = 85.201(8)$ Å^3 for FeAl-free phase D. Results from XRD, Raman spectroscopy, and EMPA demonstrate that the recovered products are pure phases without detectable impurities such as bridgmanite or stishovite as reported previously in the literatures [*Litasov et al*., 2008; *Xue et al*., 2008; *Chang et al*., 2013]. A large single-crystal FeAl-bearing sample polished on both sides was examined using conventional Mössbauer spectroscopy in transmission mode using a high specific activity ^{57}Co point source in a Rh matrix. The Mössbauer spectrum of FeAl-bearing phase D shows two well-resolved quadrupole doublets attributed to a ferrous (IS = 0.99(1) mm/s and QS = 2.34(2) mm/s) and a ferric (IS = 0.38(1) mm/s and QS = 0.61(2) mm/s) component, where the $\sum Fe^{3+}/Fe$ ratio is 0.40(5) (supporting information Figure S1). A Cameca NanoSIMS 50 L at the Carnegie Institute of Washington was used in an attempt to measure water content. However, the water content of the sample was outside the range of the standards (all basaltic glass, maximum 6.6 wt % H_2O). Therefore, we estimated the water content of two samples based on a mass and charge balance calculation from EMPA results: ~14.4 wt % for the FeAl-free sample and ~13.3 wt % for the FeAl-bearing sample.

Combined with EMPA and MS results, the chemical formula of FeAl-bearing phase D is determined to be $Mg_{0.89}Fe_{0.11}Al_{0.37}Si_{1.55}H_{2.65}O_6$, and FeAl-free phase D is $Mg_{1.14}Si_{1.73}H_{2.81}O_6$.

2.2. High-Pressure Synchrotron XRD and NFS Experiments

Symmetrical diamond anvil cells with 200 μm diameter flat culets and 150 μm diameter beveled culets were employed to achieve high pressure. Holes 100–120 μm in diameter were drilled in the preindented rhenium gasket sample chamber of ~30 μm thickness. Single-crystal samples were polished on both sides down to ~10 μm thickness using 3M™ diamond lapping films. The polished sample was loaded into the sample chamber along with Pt foil for pressure calibration [*Fei et al*., 2007]. Neon was used as the pressure medium in the FeAl-free phase D experiment, while helium was used as the pressure medium for the FeAl-bearing sample. Both ultrahigh pure Ne and He were loaded using the high-pressure gas loading system in the Mineral Physics Laboratory of the University of Texas at Austin. In situ high-pressure single-crystal XRD experiments were conducted at 13IDD beamline (GSECARS) of the Advanced Photon Source (APS), Argonne National Laboratory (ANL). A monochromatic X-ray beam with wavelength of 0.3344 Å was focused on a $5 \times 5\ \mu m^2$ spot. XRD patterns were recorded with a MarCCD detector with exposure time of 6 s where the DAC was rotated from −10° to +10° about the X-ray beam direction. The FeAl-bearing sample was under compression up to 23.8 GPa in run 1 and 110 GPa in run 2, and the FeAl-free sample was compressed up to 79 GPa in run 3. The *d* spacings of independent hkl planes (011), (110), (002), (111), (021), (121), (032), (221), (131), and (222) at various pressures were extracted by the GSE_ADA software packages [*Dera et al*., 2013], and then the unit-cell parameters were refined using UnitCell software [*Holland and Redfern*, 1997].

In situ high-pressure NFS experiments were performed using a monochromatic X-ray beam with energy of 14.4125 KeV and bandwidth of 2 meV to excite the nuclear resonance of ^{57}Fe nuclei at 16IDD beamline (HPCAT) of APS, ANL. The focused X-ray beam size was reduced to 30 μm diameter by a pinhole. Spectra were recorded by an avalanche photo diode (APD) detector in the forward direction. Diamond anvil culets of 250 μm diameter were used, and a 150 μm diameter hole was drilled in the preindented 34 μm rhenium gasket with an initial thickness of 250 μm as the sample chamber. The single-crystal phase D with dimensions of approximately $60 \times 50 \times 17\ \mu m^3$ was loaded into the sample chamber, as well as two small ruby spheres for pressure calibration [*Mao et al*., 1986]. Ne was the pressure-transmitting medium. The spectra were collected in ~5 GPa steps from ambient pressure to 71 GPa. We also measured the NFS spectra of the sample of run 2 in XRD on decompression from 110 GPa to 88 GPa. At all measured pressures, one 10 μm thick stainless steel foil was used as a reference to obtain the iron isomer shift (IS) in the sample. All NFS spectra were analyzed to extract hyperfine parameters of iron using CONUSS software [*Sturhahn*, 2000].

3. Results

3.1. NFS Results

Synchrotron NFS spectra of single-crystal FeAl-bearing phase D were collected up to 110 GPa at room temperature. Representative spectra are plotted in Figure 1. At ambient conditions, the spectrum shows three quantum beats (Figure 1a), which can be well fitted by a two-doublet model assigned to a ferrous (doublet 1, QS = 2.167(2) mm/s) and a ferric (doublet 2, QS = 0.76(2) mm/s) component, consistent with those of conventional Mössbauer spectroscopy (Figure S1 in the supporting information). Upon compression, the intensities of two of the beats (around 80 ns and 110 ns) decrease, then change significantly at 37 GPa, and finally disappear at 46 GPa. New quantum beats whose intensities become stronger with increasing pressure appear around 70 ns and 100 ns at 51 GPa (Figure 1). This behavior indicates that the electronic structure of iron in phase D undergoes a two-stage change.

We fitted spectra to obtain hyperfine parameters of iron and its relative abundances at various pressures (Figures 2 and S2 and Table S1). At pressures below 35 GPa, doublet 1 with QS of 1.96–2.34 mm/s and IS of 1.09–1.25 mm/s is assigned to the Fe^{2+}(HS) site, and doublet 2 with QS of 0.61–0.82 mm/s and IS of 0.21–0.38 mm/s is assigned to the Fe^{3+}(HS) site (Figure 2). At $35 < P < 44$ GPa, IS of some Fe^{2+} sharply decreases of ~0.5 mm/s and its QS becomes zero, consistent with a HS-to-LS transition of Fe^{2+}. Above 54 GPa, the NFS spectra are best resolved with three sites of iron (singlet 1, doublet 2a, and doublet 2b). We assigned singlet 1 with QS = 0 mm/s to Fe^{2+}(LS) derived from Fe^{2+}(HS) and doublet 2a and doublet 2b with larger QS to Fe^{3+}(LS)-I and Fe^{3+}(LS)-II, respectively, based on observations that QS sharply increases

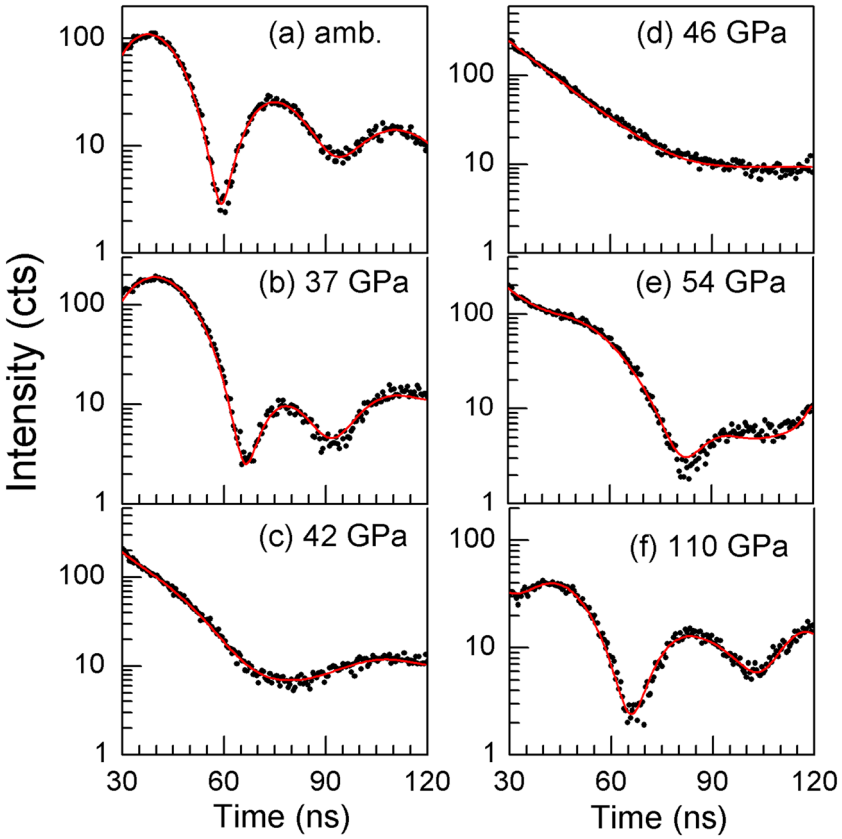

Figure 1. Representative synchrotron nuclear forward scattering spectra of FeAl-bearing phase D at high pressure and room temperature. Black solid squares are experimental data and red curves are simulated spectra.

at the HS-to-LS crossover of Fe^{3+} in octahedral coordination [*Lin et al.*, 2013]. In addition, the relative abundance constrains the two sites with larger QS from the Fe^{3+} component to keep a constant $\sum Fe^{3+}/Fe$ ratio as a function of pressure (Figure S2). We did not observe two sites for Fe^{3+}(HS) at pressures below 35 GPa, unlike at pressures above 54 GPa where two sites for Fe^{3+}(LS) were observed, suggesting that local environments of Fe^{3+} may undergo significant changes, possibly accompanying the change of the property of hydrogen bond (see further information in section 4).

3.2. XRD Results

FeAl-free and FeAl-bearing phase D samples were compressed at room temperature to pressures up to 80 and 110 GPa, respectively. The refined lattice constants of phase D at various pressures are listed in Tables S2 and S3. The unit-cell volume of FeAl-free phase D monotonously decreases with increasing pressure, while for FeAl-bearing phase D there are two marked discontinuities of ~1.7% at 37–41 GPa and ~2.0% at 64–68 GPa, respectively (Figure 3). The first discontinuity coincides with HS-LS crossover of ferrous iron (Fe^{2+}) and the second with that of ferric iron (Fe^{3+}) as supported by NFS (Figures 1 and 2). The transition pressure of the spin transition in ferric iron appears to be higher than that observed in NFS experiments, possibly due to different pressure-transmitting media (He versus Ne) and pressure calibrants (Pt versus ruby) used for the experiments. In addition, a larger pressure gradient in the sample chamber using Ne above 50 GPa could induce an earlier occurrence of the spin transition, and NFS is more sensitive for detecting changes in electronic structure compared to XRD.

We used the Birch-Murnaghan equation of state to describe the *P-V* relationship: 0.0001–37 GPa for Fe^{2+}(HS)Fe^{3+}(HS) state (denoted HS-phase D), 41–64 GPa for Fe^{2+}(LS)Fe^{3+}(HS) state (Mixed-spin phase D), and 68–110 GPa for Fe^{2+}(LS)Fe^{3+}(LS) state (denoted LS-phase D), where all parameters are summarized in Table S4, as well as previous results for comparison. Data demonstrate that the bulk modulus K_0 of phase D is

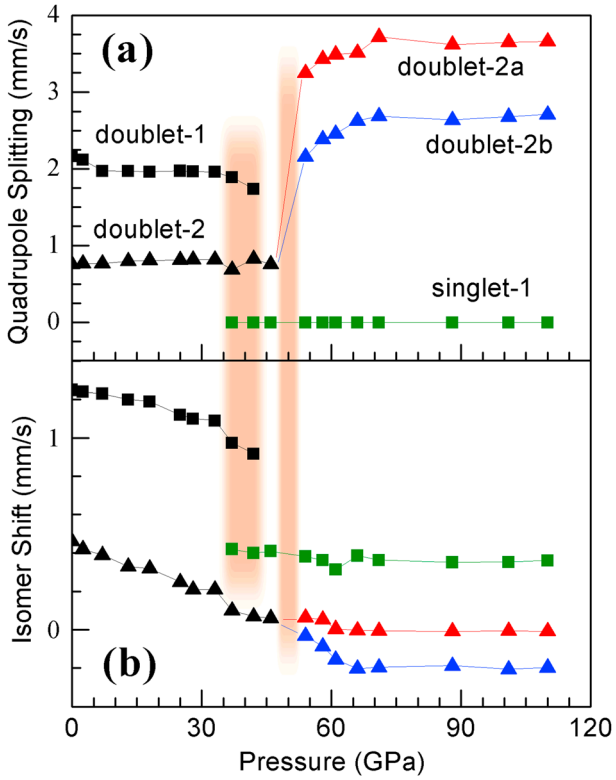

Figure 2. Hyperfine parameters of iron in FeAl-bearing phase D at high pressures across the two-stage spin transition. (a) Quadrupole splitting. (b) Isomer shift relative to α-Fe. The error bars of QS and IS are smaller than the symbols and are not shown. Black square: Fe^{2+}(HS) (boublet-1), green square: Fe^{2+}(LS) (singlet-1); black triangle: Fe^{3+}(HS) (doublet 2); and red and blue triangles: Fe^{3+}(LS) (doublet 2ab). Brown-shaded regions indicate the two-stage spin transition zones of iron in the octahedral sites.

independent of water content and the Mg/Si or $(Mg + Fe^{2+})/(Fe^{3+}+Si + Al)$ ratio (Table S4). The isothermal bulk modulus (K) of FeAl-bearing phase D can be derived through the iron spin crossover based on the method reported previously [*Wentzcovitch et al.*, 2009],

$$\frac{V}{K} = n_{LS}\frac{V_{LS}}{K_{LS}} + (1 - n_{LS})\frac{V_{HS}}{K_{HS}} - (V_{LS} - V_{HS})\left(\frac{\partial n_{LS}}{\partial P}\right)_T,$$

where K is relative to V_{HS}, V_{LS}, K_{HS}, K_{LS}, and the low-spin fraction (n_{LS}). n_{LS} can be obtained by $V = n_{LS}V_{LS} + (1 - n_{LS})V_{HS}$.

4. Discussions

4.1. Spin Transition of Iron in FeAl-Bearing Phase D

In this study, both NFS and XRD confirm that Fe^{2+} of phase D first undergoes a HS-to-LS transition at 37–41 GPa, and then Fe^{3+} undergoes the same transition at 64–68 GPa in the similar octahedral environment. The c axis of the phase D structure is incontrovertibly more compressible than the a axis, which is dominantly controlled by the MgO_6 layer, and the highly compressible nature of the c axis is coupled to the spin crossover of iron (Figure S3a). The sequence of octahedral volumes are $V(Fe^{2+}O_6) > V(MgO_6) > V(Fe^{3+}O_6)$, and thus, $Fe^{2+}O_6$ octahedra are more sensitive to pressure than those of $Fe^{3+}O_6$ along the c axis. In the sixfold coordination environment, $R(Fe^{2+} - HS)$ is larger than $R(Fe^{3+} - HS)$ by 0.13 Å [*Shannon*, 1976]. Theoretical simulations show that the crystal field stabilization energy (CFSE) of Fe^{2+} is 2.01 eV in the octahedral coordination with Fe-O bond length of 2.17 Å, while the CFSE of Fe^{3+} with Fe-O bond length of 2.06 Å is 2.66 eV [*Tossell*, 1976]. Namely, the CFSE of Fe^{2+} in phase D is smaller than that of Fe^{3+}. The results above clearly account for the sequence of the pressure-induced spin transitions of iron in phase D.

$Fe^{2+}O_6$ octahedra in MgO_6 octahedral layer of phase D are isolated without connecting by themselves but with six corner sharing by SiO_6 neighbors, whose configuration resembles those in $LiNbO_3$-type $Fe^{2+}TiO_3$ with six corner sharing and those in cubic ferropericlase with six edge sharing by themselves. At ambient conditions, IS of HS-Fe^{2+} (0.99 mm/s) in phase D is very close to that of $LiNbO_3$-type $FeTiO_3$ (1.021 mm/s) and that of ferropericlase (1.0–1.3 mm/s) [*Wu et al.*, 2010; *Lin et al.*, 2006], meaning that the s electron charge densities at the Fe^{2+} nucleus are almost the same. However QS of HS-Fe^{2+} (2.34 mm/s) in phase D is larger than that of $LiNbO_3$-type $FeTiO_3$ (1.382 mm/s) [*Wu et al.*, 2010] and that of $(Mg_{0.8},Fe_{0.2})O$ (0.8–1.0 mm/s) [*Lin et al.*, 2006], meaning that the QS of Fe^{2+} in phase D is controlled not only by next nearest neighbor oxygen atoms but also by other neighboring environments, such as the presence of OH neighbors. The spin transition pressure interval of Fe^{2+} in phase D (37–46 GPa from XRD and NFS) is smaller than that of ferropericlase (40–60 GPa), attributed to the difference of the bond length of Fe^{2+}-O (~2.02 Å in phase D versus ~2.15 Å in $(Mg_{0.8},Fe_{0.2})O$) where the larger bond length creates an internal pressure on the local Fe^{2+} ion in addition to the external pressure in a DAC [*Lin et al.*, 2006].

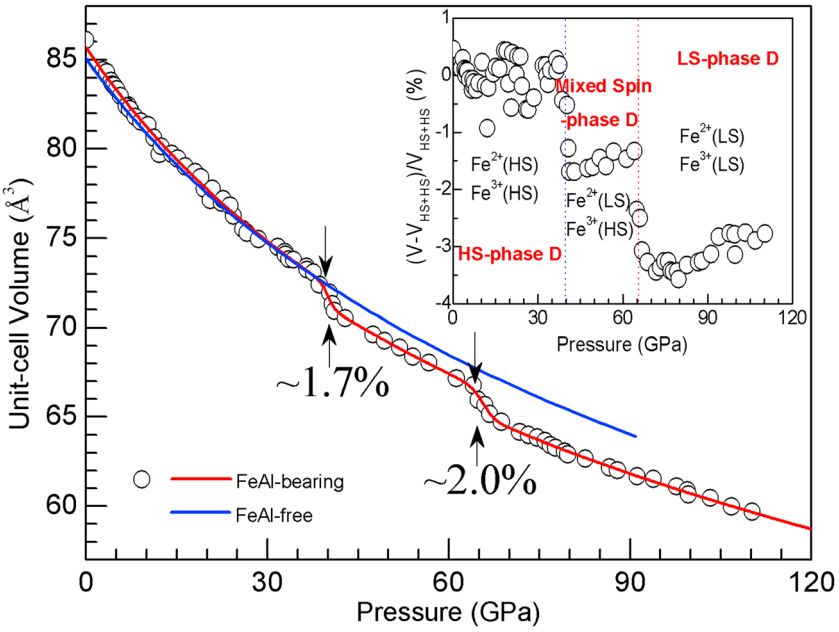

Figure 3. Unit-cell volume of phase D as a function of pressure. Open circle: experimental data of FeAl-bearing phase D; solid line: fitting results using the Birch-Murnaghan equation of state and the method from the reference [*Wentzcovitch et al*., 2009]. The volumes of both FeAl-free and FeAl-bearing phase D are almost identical at $P < 40$ GPa. In order to highlight the behavior of FeAl-bearing phase D, only the *P-V* curve (blue line) is plotted and the experimental data of FeAl-free phase D are omitted for clarity (reported in Table S2). The insert shows the volume differences (ΔV) relative to those of FeAl-bearing phase D with high-spin Fe^{2+} and Fe^{3+} state at various pressures. Both the *P-V* curve and the insert demonstrates that FeAl-bearing phase D undergoes two volume reductions, ~1.7% at ~40 GPa and ~2.0% at ~66 GPa as indicated by vertical arrows.

Based on ferric incorporation mechanisms in phase D, Fe^{3+} may occupy Mg and Si sites [*Ganskow and Langenhorst*, 2014]. One configuration that $Fe^{3+}O_6$ is located in the MgO_6 octahedral layers is similar to that of Fe^{3+} in the B site $(Mg,Fe)SiO_3$ bridgmanite, while the other is that $Fe^{3+}O_6$ is located in the SiO_6 octahedral layers resembles that in ilmenite $FeTiO_3$ or postperovskite. At ambient conditions, QS of HS-Fe^{3+} are ~0.65 mm/s for the B site Fe^{3+} in bridgmanite [*Lin et al*., 2013, and references therein] and ~0.63 mm/s for ilmenite $FeTiO_3$ [*Wu et al*., 2009], indicating that it is rather difficult to distinguish Fe^{3+} occupied in Mg or sites in the phase D case from the hyperfine parameters alone. This is the reason we only observe "one" HS-Fe^{3+} site in phase D at lower pressure (Figures 1 and 2). We note that LS-Fe^{3+} in the octahedra is known to exhibit large QS because of the ellipsoidal electronic orbitals $t_{2g}^5 e_g^0$. At pressures above 54 GPa, two clearly different local environments of Fe^{3+}(LS) are present (Figures 1 and 2). QS of doublet 2a is large but close to that of LS-Fe^{3+} in the B site of bridgmanite with six corner-sharing BO_6 octahedra in three dimensions, and QS of doublet 2b is also large but close to that of LS-Fe^{3+} in the B site postperovskite with edge/corner-sharing BO_6 octahedra in the *ac* plane [*Lin et al*., 2013, and references therein]. Thus, we can conclude that doublet 2a is the result of ~28% Fe^{3+} instead of Mg and doublet 2b is that of ~78% Fe^{3+} substitution of Si in phase D (Figures 2 and S2 and Table S1). As a general rule, the larger the QS, the more distorted the coordination polyhedron surrounding the Fe atom. We also deduce that LS $Fe^{3+}O_6$ octahedra in phase D become more distorted than those of bridgmanite and postperovskite in B sites, possibly from the effect of the next nearest neighbor hydrogen, and resulting in two distinguished components (Figure 2). The spin transition pressure interval of Fe^{3+} in phase D is very sharp (48–54 GPa from NFS and 64–68 GPa), compared with the broad interval (40–65 GPa) of FeAl-bearing Phase D ($\Sigma Fe^{3+}/Fe = 94\%$) reported by *Chang et al*. [2013], but similar to that of Fe^{3+} in the B site of bridgmanite (53–63 GPa) [*Catalli et al*., 2010]. This kind of discrepancy may be due to different abundance of ferric iron ($\Sigma Fe^{3+}/Fe = 40\%$ in present versus 94% in previous work), pressure-transmitting media (He versus Ne) and measurement tools (NFS versus XES).

4.2. Hydrogen Bond of Phase D Under Compression

Strong evidences from theoretical simulations and experimental characterizations demonstrate that pressure-induced hydrogen bond symmetrization occurs in H_2O ice-X, AlOOH, and FeOOH with ordered

hydrogen position [*Aoki et al*., 1996; *Sano-Furukawa et al*., 2008; *Gleason et al*., 2013; *Xu et al*., 2013]. However, the nature of this transition remains under debate for phase D, even for the stoichiometric ideal phase D ($MgSi_2O_6H_2$). Theoretical simulations demonstrate that different hydrogen-ordering models of ideal phase D present the different behavior of the hydrogen bond under compression, i.e., asymmetrization or symmetrization up to 100 GPa [*Tsuchiya et al*., 2005; *Mainprice et al*., 2007; *Tsuchiya and Tsuchiya*, 2008]. The change of the axial compressibility of phase D, as well as those of oxyhydroxides, was previously proposed to be indicative of symmetrization of hydrogen bonds. At lower pressure, the axial compressibility of phase D is found to be anisotropic with the *c* axis being twice as compressible as the *a* axis, but at higher pressure, the *c*/*a* ratio becomes almost constant or pressure independent (Figure S3b). The critical value of pressure is in the range of 15–40 GPa as found in a series of prior experiments and this study [*Litasov et al*., 2008; *Shinmei et al*., 2008; *Hushur et al*., 2011; *Chang et al*., 2013; *Rosa et al*., 2013b]. High-precision data only from single-crystal XRD clearly show that the *c*/*a* ratio becomes constant at 25–30 GPa for FeAl-free phase D [*Rosa et al*., 2013b, this study], ~37 GPa for the FeAl-bearing sample with $\sum Fe^{3+}/Fe = 0.40$ (this study), and ~40 GPa for the FeAl-bearing sample with $\sum Fe^{3+}/Fe = 0.94$ [*Chang et al*., 2013] (Figure S3b). When the abundance of Fe^{3+} cations with smaller radius increases, the critical pressure is delayed from 25 GPa to 40 GPa. This further supports the notion that the abnormal behavior in the *c*/*a* ratio is related to the layered structure of phase D, rather than to hydrogen bond symmetrization.

A ~20% increase of K_0 is predicted for the stoichiometric phase D model with ordered hydrogen position and symmetric hydrogen bond [*Tsuchiya et al*., 2005; *Tsuchiya and Tsuchiya*, 2008]. *Hushur et al*. [2011] observed an 18% increase in K_0 in a high-pressure X-ray powder diffraction experiment of FeAl-free phase D ($MgSi_{1.7}H_{3.0}O_6$) by fitting the *P*-*V* data in different pressure ranges (0.0001–30 GPa versus 40–55.8 GPa) and proposed the presence of the hydrogen bond symmetrization at 40 GPa. However, this change was not reported in *Rosa et al*. [2013b], as well as in this study. In addition, previous infrared spectroscopy characterization does not support the existence of hydrogen bond symmetrization of FeAl-free phase D up to 42 GPa at room temperature [*Shieh et al*., 2009]. Recently, FeOOH has been reported to simultaneously undergo spin crossover of Fe^{3+} and hydrogen bond symmetrization at above 45 GPa accompanied by a large volume collapse of ~11%, where spin crossover of Fe^{3+} does induce the hydrogen bond symmetrization [*Gleason et al*., 2013; *Xu et al*., 2013]. In present study, we clearly observe a two-stage spin transition of iron in FeAl-bearing phase D on compression (Figures 1–3). In our sample of FeAl-bearing phase D, the content of Fe^{2+} (60%) is larger than that of Fe^{3+} (40%), and the cation radius of Fe^{2+}(HS) is also larger than that of Fe^{3+}(HS) in the octahedral coordination [*Shannon*, 1976]. Thus, the volume reduction driven by the spin transition of Fe^{2+} should be larger than that of Fe^{3+}. However, the unit-cell volume reduction of ~1.7% at ~40 GPa when Fe^{2+} undergoes a HS-to-LS transition is smaller than the reduction of ~2.0% at ~66 GPa when Fe^{3+} undergoes a spin transition in FeAl-bearing phase D (Figure 3). This means that a reduction in Fe^{3+} radius alone induced by a HS-to-LS transition is not a sufficient explanation for the observed volume reduction for the second volume discontinuity. In both FeOOH and FeAl-bearing phase D, Fe^{3+} occupies the octahedral site and its next nearest neighbor is hydrogen. It is thus conceivable that hydrogen bond symmetrization induced by the spin crossover of Fe^{3+} observed in FeOOH [*Gleason et al*., 2013; *Xu et al*., 2013] also occurs in FeAl-bearing phase D, which may be used to explain the second volume discontinuity of larger reduction (Figure 3). In addition, two more distorted LS $Fe^{3+}O_6$ octahedra of phase D (Figure 2) also indicate that the next nearest neighbor hydrogen significantly affects the geometry and properties of hydrogen bonds. Thus, the presence of hydrogen bond symmetrization in FeAl-bearing phase D could be induced by the spin transition of Fe^{3+} under compression. However, future direct evidence on the hydrogen position in the lattice across the spin transition is still needed to confirm this hypothesis. We should further note that in contrast to H_2O ice and oxyhydroxides with ordered hydrogen positions, nonstoichiometric phase D with disorder hydrogen positions [*Yang et al*., 1997; *Xue et al*., 2008] makes it even more difficult to reveal the nature of the hydrogen bonds at high pressure.

4.3. Implications for the Lower Mantle

Subducting slabs have been proposed to be transporters of large quantities of Fe and Al to the deep Earth in which Al can strongly partition into hydrous phases, such as phase D and phase H, relative to coexisting bridgmanite [*Nishi et al*., 2014; *Ohira et al*., 2014]. Indeed, phase D was observed to occur in a pyrolite composition along cold thermal subduction regimes but was found to transform to an assemblage of phase

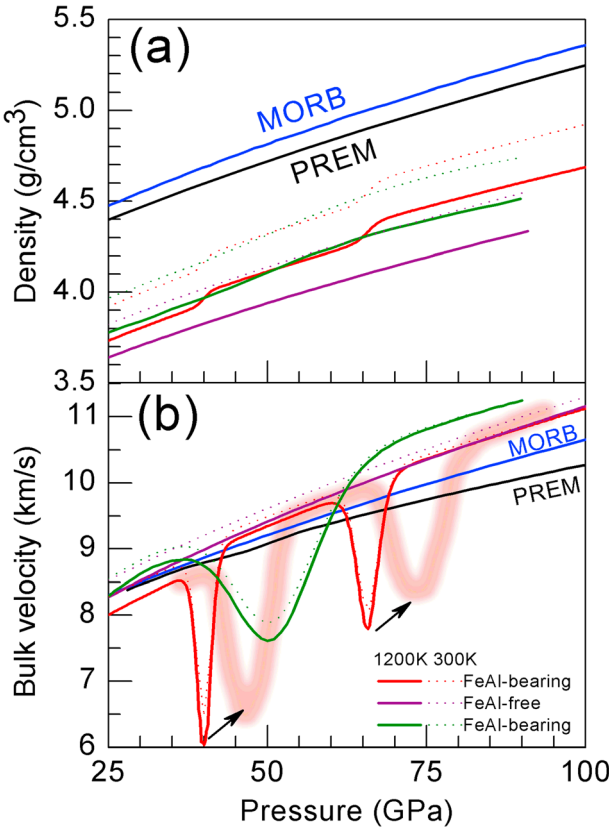

Figure 4. Density and bulk sound velocity profiles of phase D along 300 K and 1200 K isotherm at lower mantle pressures. Velocity and density profiles of MORB at 2000 K (blue line) [*Ricolleau et al.*, 2010] and PREM (black line) [*Dziewonski and Anderson*, 1981] are also plotted for comparison. Green line: $MgFe_{0.15}Al_{0.09}Si_{1.75}H_{2.51}O_6$ with $\Sigma Fe^{3+}/Fe = 0.94$ [*Chang et al.*, 2013]; red line: $Mg_{0.89}Fe_{0.11}Al_{0.37}Si_{1.55}H_{2.65}O_6$ with $\Sigma Fe^{3+}/Fe = 0.40$; violet line: $Mg_{1.14}Si_{1.73}H_{2.81}O_6$ (this study). Dotted lines represent those at 300 K, and solid lines represent those at 1200 K where the effect of high temperature is not considered on the pressure range of iron spin crossover. The profile of bulk sound velocity at 1200 K (yellow-pink thicker curve) is modeled assuming that high-temperature FeAl-bearing phase D (this study) would exhibit the same manner of the spin crossover width and the V_φ variation to those of ferromagnesite and ferropericlase [*Mao et al.*, 2011; *Liu et al.*, 2014].

H and stishovite above 50 GPa with a positive Clapeyron slope of 6.4 MPa/K at 1000 K[*Tsuchiya*, 2013; *Nishi et al.*, 2014]. On the other hand, serpentine in the subducted slabs can undergo a series of dehydration reactions while sinking into the transition zone and may eventually transform into Phase D [*Irifune et al.*, 1998]. Recent experimental investigations have also shown that the dissolution of Al in phase D can effectively extend the stable range of phase D to higher *P-T* conditions relevant to that in the subducted slabs in the lower mantle conditions [*Ghosh and Schmidt*, 2014; *Pamato et al.*, 2015]. While iron components reduce the stabilizing effect of aluminum, the Al/Fe ratio in phase D is predicted to be positively correlated with its thermal stability [*Pamato et al.*, 2015]. At 32 GPa, the stability boundary of phase D with Al/Fe ratio of 0.5–1.0 is between 1350°C and 1400°C [*Ghosh and Schmidt*, 2014]. Our FeAl-bearing sample with a higher Al/Fe ratio of 3.4 is estimated to have a higher *P-T* stability boundary and could remain stable in the subducting slabs in the deeper parts of the lower mantle at depth below 1200 km.

To understand the geophysical and geodynamic significance of our results in a subducted slab [*Lin et al.*, 2013], we have evaluated ρ and V_φ profiles of phase D as a function of pressure along a 300 K and 1200 K isotherm. Since high *P-T* EoS parameters for phase D are currently not well understood, here we assume that the spin crossover and thermal EoS behavior of phase D are similar to those of well-documented behavior of ferropericlase and ferromagnesite at high *P-T* [*Mao et al.*, 2011; *Liu et al.*, 2014] (see supporting information for details) (Figure 4). Our modeled results show that the density profiles of FeAl-bearing and FeAl-free phase D are much lower than those of preliminary reference Earth model (PREM) and mid-ocean ridge basalt (MORB) [*Dziewonski and Anderson*, 1981; *Ricolleau et al.*, 2010], indicating that the presence of phase D can contribute to a positive buoyancy force in subducted slabs at the uppermost lower mantle conditions (Figure 4a). However, the presence of Fe and Al increases its density by 3.0% [*Chang et al.*, 2013, this study], and the spin transitions of Fe^{2+} and Fe^{3+} further enhance the density increase by 1.5%–3.5% for phase D with $Mg_{0.89}Fe_{0.11}Al_{0.37}Si_{1.55}H_{2.65}O_6$ (Figure 4a); the combined effects would reduce the density difference between phase D and PREM. Our modeled V_φ profile of FeAl-bearing phase D exhibits two sharp softening associated with the two-stage spin transition: the first softening of ~28% maximum at 40 GPa and the second softening of ~20% maximum at 66 GPa and 300 K (Figure 4b). Phase D with intrinsic anisotropy of ~18% is proposed to be a possible cause of the seismic anisotropy within the deep-subducted slabs, such as Tonga, Kuril, and Izu-Bonin slabs in the transition zone and uppermost lower mantle (called "the midmantle") [*Rosa et al.*, 2013a; *Nowacki et al.*, 2015]. However, a very high volumetric fraction of phase D is required to

explain these seismic observations, indicating that phase D is unlikely a primary contributor [*Mohiuddin et al*., 2015]. The large softening in V_φ of FeAl-bearing phase D associated with the spin crossover of iron remains difficult to be used to explain the anisotropy of the midmantle because the first critical pressure range (40–55 GPa at 1200 K) corresponds to the depth of ~1100–1400 km which is shallower than that of the midmantle. But the middle-lower mantle (~1100–1800 km) beneath the circum-Pacific regions shows small-scale seismic heterogeneities whose scattered wave amplitudes range from 1 to 10% of the direct *P* waves and shows slow shear wave velocity anomalies on the order of 1–4% [*Kaneshima and Helffrich*, 2010]. These scatters are proposed to be remnants of subducted and folded former oceanic crusts which preceded the current subduction of the Pacific Plate [*Kaneshima and Helffrich*, 2010]. A simple calculation assuming LS-phase D in the subducted MORB suggests that a volumetric percentage of 7% can produce a 2% reduction in the V_φ at the depth of ~1200 km. Considering the combined effects of spin transition of Fe^{2+}, high elastic anisotropy [*Mainprice et al*., 2007; *Tsuchiya and Tsuchiya*, 2008] and deformation [*Rosa et al*., 2013a] of FeAl-bearing phase D, it is likely that only a smaller volume fraction of phase D is sufficient to cause seismic anisotropy and heterogeneity in the subducted MORB that can help explain seismic observations in the middle-lower mantle beneath the circum-Pacific area [*Lawrence and Wysession*, 2006; *Kaneshima and Helffrich*, 2010]. Together with recent experimental results that the presence of the low-spin NAL phase with a volume percentage of 20% can produce the bulk velocity reduction of the MORB assemblage by 1.8% at 41 GPa and 300 K [*Wu et al*., 2016], we propose that the spin transition of iron in the subducted MORB materials should be considered as an important source of small scattering objects at the depths of 1100–1800 km.

Acknowledgments

Synchrotron radiation X-ray measurements were performed at GSECARS and HPCAT of the APS, ANL. HPCAT operations are supported by DOE-NNSA under award DE-NA0001974 and DOE-BES under award DE-FG02-99ER45775. This research used resources of the Advanced Photon Source and a U.S. Department of Energy (DOE) Office of Science User Facility operated for the DOE Office of Science by Argonne National Laboratory under contract DE-AC02-06CH11357. X. Wu acknowledges financial support from the National Science Foundation of China (U1232204 and 41473056). J.F. Lin acknowledges financial support from the U.S. National Science Foundation. We thank Jing Yang for help in EMPA experiments and also thank Jun Tsuchiya for the nice suggestions. The data for this paper are available by contacting the corresponding authors (X. Wu: wuxiang@cug.edu.cn and J.F. Lin: afu@jsg.utexas.edu) upon request.

References

Aoki, K., H. Yamawaki, M. Sakashita, and H. Fujihisa (1996), Infrared absorption study of the hydrogen-bond symmetrization in ice to 110 GPa, *Phys. Rev. B*, *54*, 15,673–15,677.

Catalli, K., S. H. Shim, V. B. Prakapenka, J. Zhao, W. Sturhahn, P. Chow, Y. Xiao, H. Liu, H. Vynn, and W. J. Evans (2010), Spin state of ferric iron in $MgSiO_3$ perovsktie and its effect on elastic properties, *Earth Planet. Sci. Lett.*, *289*, 68–75.

Chang, Y. Y., et al. (2013), Spin transition of Fe^{3+} in Al-bearing phase D: An alternative explanation for small-scale seismic scatters in the mid-lower mantle, *Earth Planet. Sci. Lett.*, *382*, 1–9.

Dera, P., K. Zhuravlev, V. Prakapenka, M. L. Rivers, G. J. Finkelstein, O. Grubor-Urosevic, O. Tschauner, S. M. Clark, and R. T. Downs (2013), High pressure single-crystal micro X-ray diffraction analysis with GSE_ADA/RSV software, *High Pressure Res.*, *33*, 466–484.

Dziewonski, A., and D. L. Anderson (1981), Preliminary reference Earth model, *Phys. Earth Planet. Inter.*, *25*, 297–356.

Faccenda, M. (2014), Water in the slab: A trilogy, *Tectonophysics*, *614*, 1–30.

Fei, Y., A. Ricolleau, M. Frank, K. Mibe, G. Shen, and V. Prakapenka (2007), High-pressure geoscience special feature: Toward an internally consistent pressure scale, *Proc. Natl. Acad. Sci. U.S.A.*, *104*, 9182–9186.

Ganskow, G., and F. Langenhorst (2014), Stability and crystal chemistry of iron-bearing dense hydrous magnesium silicates, *Chem. Erde*, *74*, 489–496.

Ghosh, S., and M. W. Schmidt (2014), Melting of phase D in the lower mantle and implications for recycling and storage of H_2O in the deep mantle, *Geochim. Cosmochim. Acta*, *145*, 72–88.

Gleason, A. E., C. E. Quiroga, A. Suzuki, R. Pentcheva, and W. L. Mao (2013), Symmetrization driven spin transition in ε-FeOOH at high pressure, *Earth Planet. Sci. Lett.*, *379*, 49–55.

Guo, X., and T. Yoshino (2013), Electrical conductivity of dense hydrous magnesium silicates with implication for conductivity in the stagnant slab, *Earth Planet. Sci. Lett.*, *369–370*, 239–247.

Hirschmann, M. M. (2006), Water, melting, and the deep Earth H_2O cycle, *Annu. Rev. Earth Planet. Sci.*, *34*, 629–653.

Holland, T. J. B., and S. A. T. Redfern (1997), Unit cell refinement from powder diffraction data: The use of regression diagnostics, *Mineral. Mag.*, *61*, 65–77.

Hushur, A., M. H. Manghnani, and J. R. Smyth (2011), Hydrogen bond symmetrization and equation of state of phase D, *J. Geophys. Res.*, *116*, B06203, doi:10.1029/2010JB008087.

Irifune, T., K. Kuroda, N. Funamori, Y. Uchida, T. Yagi, T. Inoue, and N. Miyajima (1998), Amorphization of serpentine at high pressure and high temperature, *Science*, *272*, 1468–1470.

Kaneshima, S., and G. Helffrich (2010), Small scale heterogeneity in the mid-lower mantle beneath the circum-Pacific area, *Phys. Earth Planet. Inter.*, *183*, 91–103.

Lawrence, J. F., and M. E. Wysession (2006), Seismic evidence for subduction-transported water in the lower mantle, *Geophys. Monogr.*, *168*, 251–261.

Lin, J. F., A. G. Gavriliuk, V. V. Struzhkin, S. D. Jacobsen, W. Sturhahn, M. Y. Hu, P. Chow, and C. S. Yoon (2006), Pressure-induced electronic spin transition of iron in magneiowustite-(Mg,Fe)O, *Phys. Rev. B*, *73*(113107), 1–4.

Lin, J. F., S. Speziale, Z. Mao, and H. Marquardt (2013), Effects of the electronic spin transitions of iron in lower mantle minerals: Implications for deep mantle geophysics and geochemistry, *Rev. Geophys.*, *51*, 244–275, doi:10.1002/rog.20010.

Litasov, K. D., E. Ohtani, A. Suzuki, and K. Funakoshi (2007), The compressibility of Fe- and Al-bearing phase D to 30 GPa, *Phys. Chem. Miner.*, *34*, 159–167.

Litasov, K. D., E. Ohtani, Y. Nishihara, A. Suzuki, and K. Funakoshi (2008), Thermal equation of state of Al- and Fe-bearing phase D, *J. Geophys. Res.*, *113*, B08205, doi:10.1029/2007JB004937.

Liu, J., J. F. Lin, Z. Mao, and V. B. Prakapenka (2014), Thermal equation of state and spin transition of magnesiosiderite at high pressure and temperature, *Am. Mineral.*, *99*, 84–93.

Mainprice, D., Y. L. Page, J. Rodgers, and P. Jouanna (2007), Predicted elastic properties of the hydrous D phase at mantle pressures: Implications for the anisotropy of subducted slabs near 670-km discontinuity and in the lower mantle, *Earth Planet. Sci. Lett.*, *259*, 283–296.

Mao, H. K., J. Xu, and P. M. Bell (1986), Calibration of the ruby pressure gauge to 800-kbar under quasi-hydrostatic conditions, *J. Geophys. Res.*, *91*, 4673–4676, doi:10.1029/JB091iB05p04673.
Mao, Z., J. F. Lin, J. Liu, and V. B. Prakapenka (2011), Thermal equation of state of lower-mantle ferropericlase across the spin crossover, *Geophys. Res. Lett.*, *38*, L23308, doi:10.1029/2011GL049915.
Mohiuddin, A., M. D. Long, and C. Lynner (2015), Mid-mantle seismic anisotropy beneath southwestern Pacific subduction systems and implications for mid-mantle deformation, *Phys. Earth Planet. Int.*, *245*, 1–14.
Nestola, F., and J. R. Smyth (2016), Diamonds and water in the deep Earth: A new scenario, *Int. Geol. Rev.*, *58*, 263–276.
Nishi, M., T. Irifune, J. Tsuchiya, Y. Tange, Y. Nishihara, K. Fujino, and Y. Higo (2014), Stability of hydrous silicate at high pressures and water transport to the deep lower mantle, *Nat. Geosci.*, *7*, 224–227.
Nowacki, A., J. M. Kendall, J. Wookey, and A. Pemberton (2015), Mid-mantle anisotropy in subduction zones and deep water transport, *Geochem. Geophys. Geosyst.*, *16*, 764–784, doi:10.1002/2014GC005667.
Ohira, I., E. Ohtani, T. Sakai, M. Miyahara, N. Hirao, Y. Ohishi, and M. Nishijima (2014), Stability of a hydrous δ-phase, AlOOH-$MgSiO_2(OH)_2$, and a mechanism for water transport into the base of lower mantle, *Earth Planet. Sci. Lett.*, *401*, 12–17.
Pamato, M. G., R. Myhill, T. B. Ballaran, D. J. Frost, F. Heidelbach, and N. Miyajima (2015), Lower-mantle water reservoir implied by the extreme stability of a hydrous aluminosilicate, *Nat. Geosci.*, *8*, 75–79.
Pearson, D. G., et al. (2014), Hydrous mantle transition zone indicated by ringwoodite included within diamond, *Nature*, *507*, 221–224.
Ricolleau, A., J. P. Perrillat, G. Fiquet, I. Daniel, J. Matas, A. Addad, N. Menguy, H. Cardon, M. Mezouar, and N. Guignot (2010), Phase relations and equation of state of a natural MORB: Implications for the density profile of subducted oceanic crust in the Earth's lower mantle, *J. Geophys. Res.*, *115*, B08202, doi:10.1029/2009JB006709.
Rosa, A. D., C. Sanchez-Valle, and S. Ghosh (2012), Elasticity of phase D and implication for the degree of hydration of deep subducted slabs, *Geophys. Res. Lett.*, *39*, L06304, doi:10.1029/2012GL050927.
Rosa, A. D., C. Sanchez-Valle, C. Nisr, S. R. Evans, R. Debord, and S. Merkel (2013a), Shear wave anisotropy in textured phase D and constraints on deep water recycling in subduction zones, *Earth Planet. Sci. Lett.*, *377–378*, 13–22.
Rosa, A. D., M. Mezouar, G. Garbarino, P. Bouvier, S. Ghosh, and C. Sanchez-Valle (2013b), Single-crystal equation of state of phase D to lower mantle pressures and the effect of hydration on the buoyancy of deep subducted slabs, *J. Geophys. Res. Solid Earth*, *B118*, 6124–6133, doi:10.1002/2013JB010060.
Sano-Furukawa, A., K. Komatsu, C. B. Vanpeteghem, and E. Ohtani (2008), Neutron diffraction study of δ-AlOOD at high pressure and its implication for symmetrization of the hydrogen bond, *Am. Mineral.*, *93*, 1558–1567.
Shannon, R. D. (1976), Revised effective ionic radii and systematic studies of interatomic distances in halides and chalcogenides, *Acta Crystallogr. Sect. A*, *32*, 751–767.
Shieh, S. R., H. K. Mao, R. J. Hemley, and L. C. Ming (1998), Decomposition of phase D in the lower mantle and the fate of dense hydrous silicates in subducting slabs, *Earth Planet. Sci. Lett.*, *159*, 13–23.
Shieh, S. R., T. S. Duffy, Z. Liu, and E. Ohtani (2009), High-pressure infrared spectroscopy of the dense hydrous magnesium silicates phase D and phase E, *Phys. Earth Planet. Inter.*, *175*, 106–114.
Shinmei, T., T. Irifune, T. Tsuchiya, and F. Funakoshi (2008), Phase transition and compression behavior of phase D up to 46 GPa using mulit-anvil apparatus with sintered diamond anvils, *High Pressure Res.*, *28*, 363–373.
Sturhahn, W. (2000), CONUSS and PHOENIX: Evaluation of nuclear resonant scattering data, *Hyperfine Interact.*, *125*, 149–172.
Tossell, J. A. (1976), Electronic structures of iron-bearing oxidic minerals at high pressure, *Am. Mineral.*, *61*, 130–144.
Tsuchiya, J. (2013), First principles prediction of a new high-pressure phase of dense hydrous magnesium silicates in the lower mantle, *Geophys. Res. Lett.*, *40*, 4570–4573, doi:10.1002/grl.50875.
Tsuchiya, J., and T. Tsuchiya (2008), Elastic properties of phase D ($MgSi_2O_6H_2$) under pressure, *Phys. Earth Planet. Int.*, *170*, 215–220.
Tsuchiya, J., T. Tsuchiya, and S. Tsuneyuki (2005), First-principles study of hydrogen bond symmetrization of phase D under high pressure, *Am. Mineral.*, *90*, 44–49.
Wentzcovitch, R., J. Justo, Z. Wu, C. R. da Silva, D. Yuen, and D. Kohlstedt (2009), Anomalous compressibility of ferropericlase throughout the iron spin cross-over, *Proc. Natl. Acad. Sci. U.S.A.*, *106*, 8447–8452.
Wu, X., G. Steinle-Nemann, O. Narygina, I. Kantor, C. McCammon, S. Pascarelli, G. Aquilanti, V. Prakapenka, and L. Dubrovinsky (2009), Iron oxidation state of $FeTiO_3$ under high pressure, *Phys. Rev. B*, *79*(094106), 1–7.
Wu, X., G. Steinle-Nemann, O. Narygina, C. McCammon, and L. Dubrovinsky (2010), In situ high-pressure study of $LiNbO_3$-type $FeTiO_3$: X-ray diffraction and Mössbauer spectroscopy, *High Pressure Res.*, *30*, 395–405.
Wu, Y., X. Wu, J. F. Lin, C. A. McCammon, Y. Xiao, P. Chow, V. B. Prakapenka, T. Yoshino, S. Zhai, and S. Qin (2016), Spin transition of ferric iron in the NAL phase: Implications for the seismic heterogeneities of subducted slabs in the lower mantle, *Earth Planet. Sci. Lett.*, *434*, 91–100.
Xu, W., et al. (2013), Pressure-induced hydrogen bond symmetrization in iron oxyhydroxide, *Phys. Rev. Lett.*, *111*, 175501.
Xue, X., M. Kanzaki, and A. Shatshiy (2008), Dense hydrous magnesium silicates, phase D, and superhydrous B: New structural constraints from one- and two-dimensional ^{29}Si and ^{1}H NMR, *Am. Mineral.*, *93*, 1099–1111.
Yang, H., C. T. Prewitt, and D. J. Frost (1997), Crystal structure of the dense hydrous magnesium silicate, phase D, *Am. Mineral.*, *82*, 651–654.